



CELL-INTEGRATED SENSING FUNCTIONALITIES FOR SMART BATTERY SYSTEMS
WITH IMPROVED PERFORMANCE AND SAFETY

GA 957273

D3.1 REPORT ON ADAPTATION OF LEVEL 1 SENSORS FOR
INCORPORATION INTO BATTERY CELLS

LC-BAT-13-2020 - Sensing functionalities for smart battery cell chemistries



| | | |
|----------------------------|--|------------|
| Deliverable No. | 3.1 | |
| Related WP | 3 | |
| Deliverable Title | Report on adaptation of level 1 sensors for incorporation into battery cells | |
| Deliverable Date | 28-02-2022 | |
| Deliverable Type | REPORT | |
| Dissemination level | Public (PU) | |
| Written By | Vincent Dreher (FHG) | 15-02-2022 |
| | Dr. Michael Jank (FHG) | 15-02-2022 |
| Checked by | Harald Kren (VAR) | 23-02-2022 |
| Reviewed by | Iñigo Gandiaga (IKE) | 23-02-2022 |
| | Harald Kren (VAR) | 23-02-2022 |
| Approved by | Iñigo Gandiaga (IKE) | 28-02-2022 |
| Status | Final | 28-02-2022 |



Summary

SENSIBAT uses two instances of sensors for derivation of relevant physico-chemical parameters in situ, i.e. inside the battery cells. The integration with the battery electrode stack demands for a flexible thin-film electronics approach. Level 1 sensors under consideration in task 3.1 focus on proven sensing principles and arrange temperature and pressure sensors in a matrix style that allows the read out with spatial resolution. The goals of the sensor adaptation process are:

- Selection of appropriate sensing principles and materials to fulfil the requirements stated in deliverable 1.1
- Definition of sensor devices, layouts and layer stacks
- Sampling of test devices and assessment of materials and layouts
- Integration of an appropriate addressing system and respective wiring architecture with the sensors on one side and the battery management system (electronic read out) on the other

In order to fulfil the tasks, resistive temperature sensor and parallel-plate capacitors based on pressure-sensitive insulators have been under investigation. For temperature sensors three thin-film metals were analysed of which platinum and a nickel-aluminium alloy gave the best performance with respect to temperature sensitivity, linearity and hysteresis. Out of a variety of polymeric materials, polyurethane yields sufficient mechanical and electrical responses for integration with the pressure sensors.

The addressing scheme matching the components was jointly set up with SENSIBAT colleagues responsible for the battery management electronics. Aiming at a reduction of the number of wiring lines, the temperature sensors will be read out in a cross-point arrangement whereas the capacitive sensors use a common ground/common rail approach. A respective layout has been developed and was the basis for the manufacturing of prototype samples.

Parallel developments considering the encapsulation of the sensing matrix against the influence of the battery electrolyte revealed the need for a high-temperature anneal that could not be applied to the polyurethane projected for use as pressure sensitive element. Thus, a follow-up activity aiming at a replacement of the insulator in the pressure sensors has been started and is scheduled to be available for realization of the final SENSIBAT level 1 sensor sheets.

There are no deviations from the description of this deliverable as given in Annex I of the Grant Agreement.



Table of Contents

| | | |
|-------|---|----|
| 1 | Introduction | 7 |
| 2 | Technical Report | 9 |
| 2.1 | Overview over requirements for level 1 sensors..... | 9 |
| 2.1.1 | Requirements for the temperature sensors (Point 4.2 in D1.1)..... | 9 |
| 2.1.2 | Requirements for the pressure sensors (Point 4.3 in D1.1)..... | 9 |
| 2.2 | Adaptation of the temperature sensor..... | 9 |
| 2.3 | Adaptation of the pressure sensor..... | 14 |
| 2.3.1 | Materials choice and mechanical considerations..... | 14 |
| 2.4 | Integrated processing of temperature and pressure sensors..... | 21 |
| 2.4.1 | Process flow..... | 21 |
| 2.4.2 | Wiring of sensor matrix | 21 |
| 3 | Discussion & Conclusion | 24 |
| 4 | Risks | 25 |
| 5 | References | 26 |
| 6 | Acknowledgement | 27 |



Table of Figures

| | |
|--|----|
| Figure 1: Temperature sensors on silicon carrier based on existing layout during I-V measurement..... | 10 |
| Figure 2: Normalized sensor resistances of six different samples at different temperatures..... | 10 |
| Figure 3: Difference of calculated TCR based on heating and cooling curve for the three sensor materials before and after annealing at 300 °C in nitrogen atmosphere..... | 11 |
| Figure 4: Single temperature sensor (NiAl) connected with crimp plug..... | 12 |
| Figure 5: Normalized resistance of NiAl based temperature sensors on PI-substrate in a climate chamber between -20 and 110 °C..... | 13 |
| Figure 6: Comparison of the fracture toughness and Young's modulus values of polymers with other materials. ^[2] | 15 |
| Figure 7: Initial measurement setup and results of PU-based pressure sensor characterisation under small loads. | 16 |
| Figure 8: Advanced measurement setup and affiliated results for capacitive pressure sensors under higher loads. | 16 |
| Figure 9: Photograph and SEM picture of NuSil dielectric on silicon substrate after initial optimisation of spin-coating process..... | 17 |
| Figure 10: Photograph of test structures for pressure dependent characterisation based on Sylgard silicone (left) and SEM picture with thickness measurement of Sylgard on silicon wafer (right). | 18 |
| Figure 11: leakage current measurements for 9 NuSil capacitors between -3 and 3V..... | 18 |
| Figure 12: Frequency dependent measurement of the capacity of NuSil based test structures. | 19 |
| Figure 13: Voltage dependent measurement of the capacity of NuSil based test structures at different frequencies. | 19 |
| Figure 14: Equipment for initial characterisation of capacitors under pressure..... | 20 |
| Figure 15: Process flow for the manufacturing of level 1 sensor matrices. | 21 |
| Figure 16: wiring schemes for contacting individual sensors in a matrix configuration. a) Contacting each element individually by the required number of wires. b) Common rail concept where all elements share a common ground or supply line. c) Cross point matrix where each row and each line share a single wire. | 22 |
| Figure 17: Parallel current paths in crosspoint configuration demand an advanced read-out scheme. The red path shunts reading out the element addressed by the yellow lines. Note that this is only one possible shunting path..... | 23 |
| Figure 18: SENSIBAT Level 1 sensor matrix designed for 1 Ah battery cells before encapsulation. The matrix holds 12 resistive temperature sensors for cross-point array addressing as well as 12 capacitive pressure sensors in common rail configuration..... | 23 |



Abbreviations

| Symbol / Abbreviation | |
|-----------------------|---|
| A | <i>Area of capacitor</i> |
| BMS | <i>Battery Management System</i> |
| C | <i>Capacity</i> |
| d | <i>Distance between electrodes</i> |
| e_0 | <i>Vacuum permittivity</i> |
| e_r | <i>Relative permittivity</i> |
| ε | <i>Strain</i> |
| E | <i>Young's modulus</i> |
| m | <i>Number of rows in a sensor matrix</i> |
| MEMS | <i>Microelectromechanical systems</i> |
| N | <i>Total number of wires to connect a sensor matrix</i> |
| n | <i>Number of columns in a sensor matrix</i> |
| PI | <i>Polyimide</i> |
| PU | <i>Polyurethane</i> |
| PTC | <i>Positive temperature coefficient</i> |
| p-sensor | <i>Pressure sensor</i> |
| SEM | <i>Scanning electron microscope</i> |
| σ | <i>Stress</i> |
| TCR | <i>Thermal coefficient of resistance</i> |
| T-sensor | <i>Temperature sensor</i> |



1 Introduction

In general, the SENSIBAT project aims at a better understanding of battery operation modes by direct integration of sensor functionalities into the cells. Besides the investigation of novel functional electrodes allowing for analysis of the electrode and electrolyte quality by electrochemical impedance spectroscopy (*level 2* sensors), established sensing concepts for temperature and pressure sensing (so-called *level 1* sensors) are adapted for integration of the sensors with the electrode stack, i.e. inside the housing of the battery cell.

Resistive temperature sensors (T-sensor) have been demonstrated before by project partner Fraunhofer IISB and are tailored to the requirements of SENSIBAT. The heart of the sensor comprises a meander structure of the temperature sensitive material delivering a large width to length (W/L) ratio at considerably low thickness. This layout in conjunction with low resistivity wiring yields a setup that is very site specific and allows for the extraction of spatially resolved temperature distributions from dedicated sensor matrices.

The capacitive sensing principle has been successfully applied by Fraunhofer IISB for touch, fill-level, and humidity sensing in various configurations. In SENSIBAT the principle is applied for read out of capacitance changes in a polymer under compression (p-sensor). Both the thickness reduction as well as compression and respective change of permittivity lead to an increase in the capacity of a parallel plate capacitor that can be detected electrically.

An important aspect of spatially resolved sensing applications is the wiring challenge of large numbers of sensing spots in a matrix. Basically, each respective temperature and pressure sensor can be accessed by two connectors. However, taking into account an arrangement with each 3 x 4 temperature and pressure sensors for the 1 Ah cells under investigation this approach will sum up to 48 wires. In turn this will need for a considerable width of the feed through that has to be integrated with the sealant of the battery pouch. Several options to reduce the count of wires without worsening accessibility have been discussed with representatives of SENSIBAT WP4 and led to the corresponding design of the 1 Ah sensor matrix as well as the read-out system integrated with the battery-management system (BMS).

This deliverable is based on the work done in Task 3.1 and describes the development of temperature and pressure sensors with adaptation to the requirements which were set in Deliverable 1.1 "Requirement Specification (Use cases, KPIs and cell, module requirements)". The requirements of D1.1 are derived from the viewpoint of an industrial application – this document provides the information how those requirements were met and points out the limitations of the approach.

The following aspects regarding sensor adaptation will be explained within this document:

- Basic mode of operation for level 1 sensors
- Requirements set for the sensors in D1.1 and how they are addressed within the scope of Task 3.1
- Materials choices based on requirements
- Characterisation of prototypes
- Multi sensor array and derived layout

Task 3.1 "Adaptation of level 1 sensors for incorporation into battery cells" started in month 1 of the SENSIBAT project and ends in month 18. For work within other tasks, more matrices and therefore level 1 sensors will be manufactured after M18 (matrices for the 5 Ah cells, related to Task 3.4), allowing for minor adjustments within the processing and fine tuning of sensor materials and design. However, at this point in time (M18) it is crucial



for the further progression of the project to have the working principle, expected matrix dimensions, wiring and some cornerstone values regarding resistances (T-sensor) and capacitances (p-sensor) fixed. With this information a suitable read-out circuit can be build (WP4) and the cell assembly (WP3) can be adjusted to the dimensions of the matrix (especially regarding the feed-through).



2 Technical Report

2.1 Overview over requirements for level 1 sensors

In this chapter the relevant parameters and requirements for the level 1 sensor from D1.1 are summarized to give an overview of the required sensor properties [preferred values are shown in brackets].

Furthermore, the environment in the battery and the necessity that the sensors do not interfere with the ion fluxes impose a few constrictions on the sensor matrix which is developed in SENSIBAT. The sensor matrix has to be stable within the electrolyte: on one hand, nothing gets dissolved in the electrolyte which might interfere with the chemical environment of the battery, and on the other hand, no harm is done to the sensors and their wiring. Additionally, there should not be any significant topology on the matrix to reduce or prevent mechanical stress onto the electrodes/battery through the incorporation of the matrix, especially under the build-up of internal pressure during expansion of the electrode stack during charging. The matrix materials themselves have to be able to withstand a decent amount of pressure which evolves throughout the cycling of a battery; therefore, the materials involved should not be brittle. Based on these constrictions, it was chosen to process both the temperature and pressure sensor onto one substrate, which is placed either between the pouch foil and the last electrode of the cell (for rather thin cells) or between two separator foils in the centre of the electrode stack (for thicker cells). Polyimide (PI) was chosen as substrate material due to its chemical inertness, flexibility, electrical and chemical barrier properties and its high heat resistance. Additionally, it can be manufactured through a spin coating process onto silicon wafers which act as carrier during further thin-film processing. The single sensors were aimed to be flat and as simple as possible - without losing sensitivity or stability - to ensure an easy read out as well as facile processing.

2.1.1 Requirements for the temperature sensors (Point 4.2 in D1.1)

The temperature sensors shall enable a spatial resolution of at least 15 mm. The measurement range of the resulting sensor matrix should be between -20 and 60 °C [-20 - 100 °C] with an accuracy of +/- 1 °C [+/- 0,5 °C] over the whole measurement range. Furthermore, they should have a lifetime of at least 8 years without degenerated performance. Depending on the sensor integration, they shall be able to withstand temperatures of up to 140 °C if necessary, at least for a short amount of time (drying and, sealing processes).

2.1.2 Requirements for the pressure sensors (Point 4.3 in D1.1)

The pressure sensors shall enable a spatial resolution of at least 15 mm. The measurement range of the resulting sensor matrix should be between 0 and 1,5 MPa with an accuracy of +/- 1 % over the whole measurement range. Furthermore, they should have a lifetime of at least 8 years without degenerated performance. Depending on the sensor integration, they shall be able to withstand temperatures of up to 140 °C if necessary, at least for a short amount of time (drying and sealing processes).

2.2 Adaptation of the temperature sensor

Temperature sensors can be realized based on different concepts, which all have different advantages and disadvantages. Resistor-based (thermistors or PTCs in this case) temperature sensors were chosen over conductive composites and thermoelements due to their simplicity both in manufacturing (only one deposition step) and read-out (resistance measurement). Thermistors are resistors that change their electrical resistance in a predictable way when the temperature of the resistor changes. Three different materials were investigated based on reviewed literature and good availability or processability: platinum (Pt), nickel (Ni) and a nickel-alloy



with 2,6% aluminium (NiAl). Temperature sensors based on an existing layout were produced with these materials as temperature sensitive part on two silicon wafers per material and evaluated through resistance measurements on a heatable chuck (see figure 1).

The sensitive part consists of a low width-to-length ratio meander structure of thermally sensitive metal, 30-50 nm in thickness (depending on material) to ensure a high base resistance, while aluminium (supply) lines

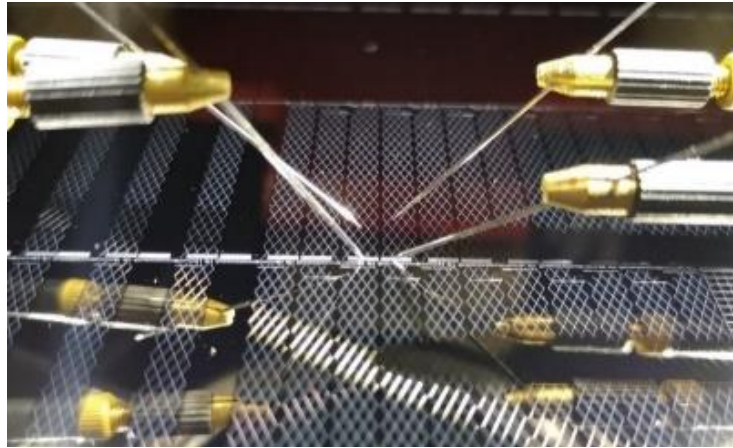


Figure 1: Temperature sensors on silicon carrier based on existing layout during I-V measurement.

which connect the sensors have a thickness of 500 nm. The resulting difference in base resistance of the temperature sensitive material and the supply lines diminishes the influence of the supply lines on the overall temperature measurement and therefore ensures that the measurement is only influenced by the locally confined temperature dependent resistor. A high base resistance is beneficial for an accurate measurement and a low power consumption.

Figure 2 shows a comparison of the three materials under investigation with respect to their resistance dependency on temperature between 30 °C and 120 °C.

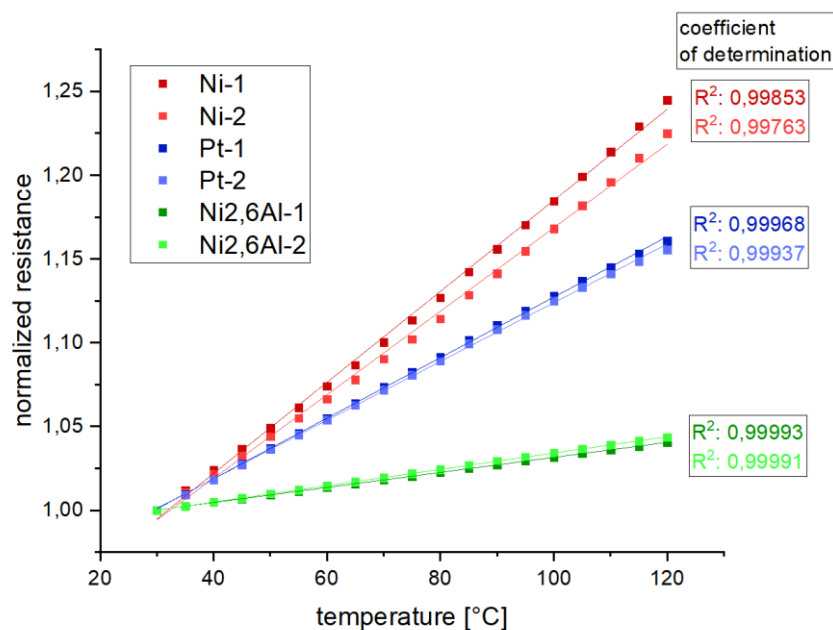


Figure 2: Normalized sensor resistances of six different samples at different temperatures.



As can be seen in figure 2 and table 1, pure Nickel (Ni) shows the highest temperature coefficient of resistance (TCR) of the three materials, but also has the highest deviation from ideal linear behaviour with an R^2 value of approximately 0,998. However, the nickel resistors showed high deviations and nonlinearity in contact and sheet resistance measurements which were performed on test structures on the two wafers.

Platinum shows a better linearity than nickel and a high TCR compared to the nickel aluminium alloy (NiAl). NiAl shows the lowest TCR of all the materials with 0,049 %/K but also the least deviations from the model. Both Pt and NiAl showed very high spatial homogeneity with respect to sheet and contact resistances (N=98).

Table 1: TCR of the temperature sensors based on the three different materials.

| TCR in | Ni-1 | Ni-2 | Pt-1 | Pt-2 | NiAl-1 | NiAl-2 |
|--------------------|-------------------------|-------------------------|-------------------------|-------------------------|-------------------------|-------------------------|
| [%/K] | 0,272 | 0,249 | 0,181 | 0,176 | 0,045 | 0,049 |
| [K ⁻¹] | 2,717 *10 ⁻³ | 2,493 *10 ⁻³ | 1,806 *10 ⁻³ | 1,757 *10 ⁻³ | 0,448 *10 ⁻³ | 0,487 *10 ⁻³ |

In order to estimate the possible influence of changes within the resistor through continuous heating and cooling, additional hysteresis measurements were conducted. The sensors were heated up in steps of 10 °C from 30 °C to 120 °C and subsequently cooled down to 30 °C again while also measuring the resistance. The TCRs were then calculated separately from the heating (30 °C → 120 °C) and cooling curve (120 °C → 30 °C), and the difference in TCR - which is an indicator for the hysteresis - was calculated.

An additional annealing step (300 °C for 1h in nitrogen atmosphere) was performed to reduce the stress and defects within the resistors and therefore reduce hysteresis and non-linearity. The measurements to calculate the heating vs. cooling curve TCR were then repeated. The comparison of the temperature sensors before and after annealing is shown in figure 3:

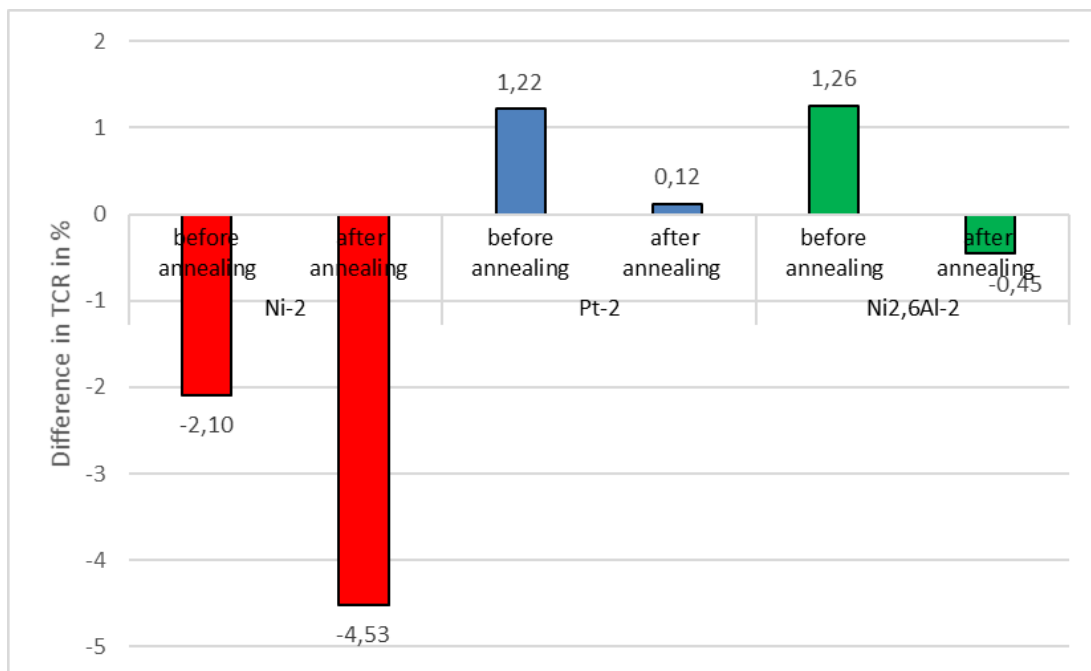


Figure 3: Difference of calculated TCR based on heating and cooling curve for the three sensor materials before and after annealing at 300 °C in nitrogen atmosphere.



Based on a reduction of the TCR by 2,1% for the cooling curve compared to the heating curve, it is evident that pure nickel shows strong non-linearity, which was even increased by the annealing. Therefore, it is not suitable as temperature sensitive material within the scope of this project. Pt and NiAl in contrary show the expected improvement of repeatability/linearity for consecutive measurements by the additional annealing step. Additionally, the TCR of the annealed NiAl sensors increased from 0,049 %/K to 0,091 %/K while the TCR of the Pt sensor was slightly reduced. Annealed platinum-based sensors show a forward/backward deviation of the TCR of 0,12 %, which might not even be solely based on the material itself, but could be influenced by inaccuracy of the measurement and especially the heating setup. Referring to the accuracy requirement of D1.1, a deviation of less than 0,5 °C is preferred. Given a calibration of the sensor at room temperature (25°C, base resistance of 10 kOhm), an error of 0,12% in the TCR (assuming TCR of 0,180%/K – 18 Ohm/K for a 10 kOhm sensor) and a real temperature of 60 °C within the cell which we want to measure, we can calculate our error in the temperature measurement: the resistance of 10 kOhm will change by $10000 \text{ Ohm} * 35 \text{ K} * 0,18 \frac{\%}{\text{K}}$ to 10,630 kOhm. If the TCR however is actually 0,12 % higher, the measured value would be: $10000 \text{ Ohm} + \left(10000 \text{ Ohm} * 35 \text{ K} * 0,180216 \frac{\%}{\text{K}} \right) = 10,6307 \text{ kOhm}$. Consequently, there is a difference of 0,7 Ohm, which introduces an error of 0,038 °C between the measured and the real value. Therefore, the expected accuracy can be easily met with the platinum based, annealed sensor. For NiAl the numbers are slightly, but the error is lower than the preferred deviation as well: 0,23°C.

Note that these sensors were not encapsulated, i.e. exposed to oxygen and humidity throughout all these measurements. We expect that sensor degradation is even less when devices are covered by diffusion-tight layers. Additionally, the temperature measurements for the calculation of these TCR values were done on a heatable chuck which itself could show temperature deviations.

As explained before, platinum shows the best overall performance of the three investigated materials. However, the nickel-aluminium alloy shows even better linearity and might offer a good economic alternative to platinum due to its comparably very low price. The lower TCR of NiAl could be compensated with a sufficiently accurate measurement circuit.

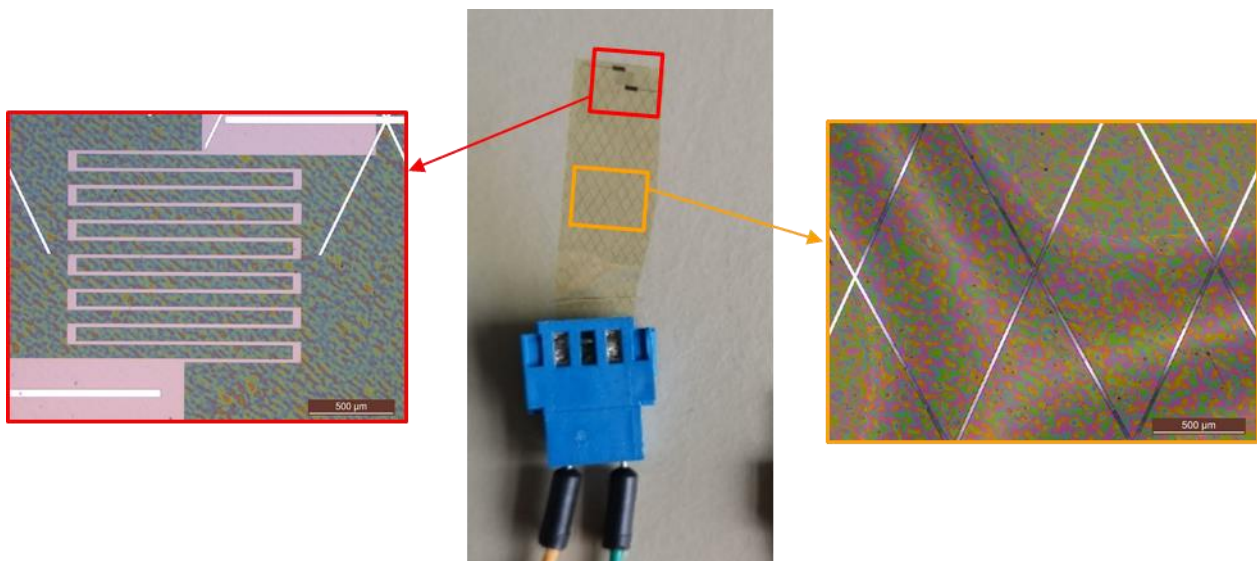


Figure 4: Single temperature sensor (NiAl) connected with crimp plug.

Further NiAl based temperature sensors were processed on polyimide (which itself was manufactured on a silicon carrier, meeting the projected manufacturing flow) to show the successful transfer from a rigid silicon



substrate onto a flexible polymer foil. Due to the lower thermal conductivity and the difficulty to mount the sensors onto the thermal chuck without air entrapment, a climate chamber instead of the heating chuck was used to control the temperature. The sensors were therefore released from the silicon carrier and crimped to enable the electrical measurement (shown in Figure 4).

Based on the results shown previously, the annealing of the sensors in nitrogen was performed under the same conditions to improve the temperature sensors.

Figure 5 shows the results of the performed measurements between -20 and 110 °C.

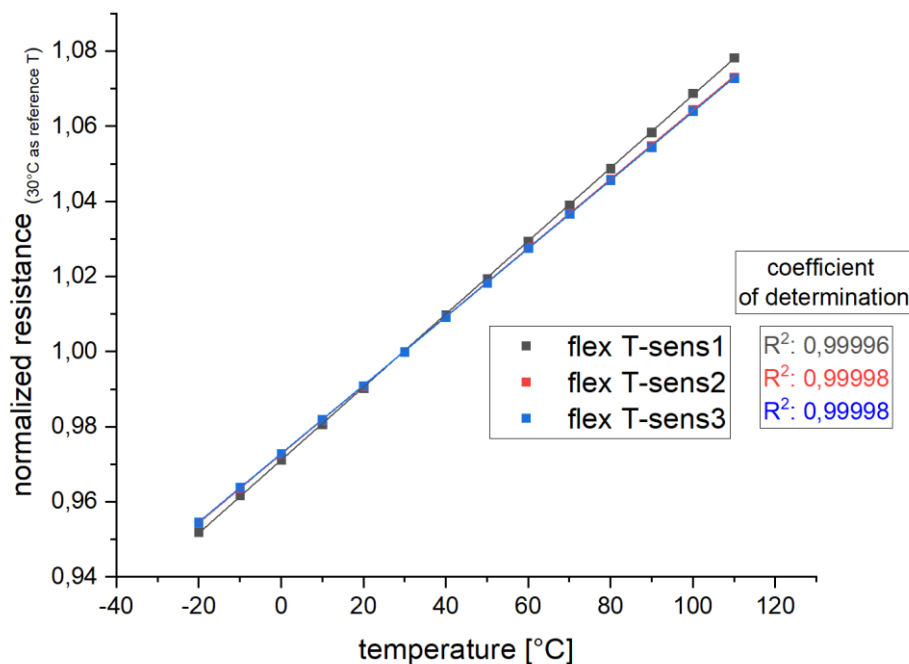


Figure 5: Normalized resistance of NiAl based temperature sensors on PI-substrate in a climate chamber between -20 and 110 °C.

With a TCR of 0,097%/K and even improved linearity ($R^2 = 0,99998$) it was shown for the NiAl based sensors that the transfer from rigid silicon substrates to a flexible PI foil yields functional, flexible and highly accurate sensors. As it is evident from the graphs of figure 5, the processed temperature sensors are also usable for the detection of negative temperatures.

Based on the measurements, it was shown that hysteresis could be reduced by a thermal treatment in nitrogen atmosphere to meet the required measurement accuracy. However, a calibration (at least two points) is always mandatory due to the different base resistances and TCRs of the single sensors, which arise due to local variations in dimensions (thickness, width of metal tracks) in the processing. Note that typical techniques applied for the definition/selection of high precision temperature sensors like binning or laser trimming are not applicable due to the contiguous processing of all sensors on a single sheet on one side and the sensors being buried under auxiliary layers (multilayer metallization, encapsulation) on the other.



2.3 Adaptation of the pressure sensor

There are different types of pressure sensors available including piezoelectric, piezoresistive and capacitive sensors. Piezoelectric pressure sensors are based on the piezoelectric effect which generates electrical voltages through the compression or extension of a material. While this type of sensor is fitting for measurements of low and dynamic pressures, it is not ideal for the monitoring of rather static and slowly developing pressures which are expected to appear within a li-ion battery cell. The main source of pressure within a battery comes from the preloading of the battery cell with a few hundred kPa and the pressure of the electrodes which dilate through intercalation of lithium ions throughout the operation of the battery. Therefore, a direct mechanical pressure from all over the electrodes onto the pressure sensors rather than a hydrostatic pressure is expected. Piezoresistive pressure sensors typically are realized through meander structures, which are placed over a membrane with a cavity below to allow the membrane to deform through pressure on the z-axis. The meander structures then act like strain gauges and increase their resistance through the deformation. But these membranes and cavities require a lavish production and typically are distinct, rigid MEMS which are not compatible with a flexible substrate. We initially also investigated into piezoresistive meander structures without cavity or membrane. However, those showed only very low responses (0,05 % resistance change between 0 and 1500 kPa) to the applied pressure. Therefore, capacitive sensors with compressible dielectrics were investigated to manufacture simple and effective pressure sensors for monitoring of static pressures within batteries.

2.3.1 Materials choice and mechanical considerations

The envisioned capacitive pressure sensors are designed in parallel-plate configuration to use the capacitance of a device either as a function of the dielectric constant of a material, the distance between two electrodes or both (see equation 1).

$$C = \epsilon_0 \epsilon_r \frac{A}{d} \quad (1)$$

Capacitive pressure sensors with porous dielectric materials show both dependencies; their dielectric constant increases due to a reduction of the porosity and due to a reduced distance between the two electrodes. Anyhow they are rather hard to manufacture and the porosity is difficult to control. They are generally more suitable to detect very low pressure changes due to their "double dependency". Therefore, typical plate capacitors with a compressible dielectric are investigated within this project.

While harder dielectrics might not show a significant compression and therefore change in capacitance within the defined pressure range (0 - 1500kPa), softer materials might deform under high pressures which can result in delamination or destruction of the capacitor plates, which are placed on the compressible dielectric. Additionally, soft materials (elastomers in specific) often show a low compression set, which means that there is a low threshold of compression which the material can recover from elastically. Above that threshold not all the deformation is reversible and a permanent deformation is induced.^[1] To keep a balance between sensitivity and endurance, calculations based on Hooke's law (equation 2) were used to estimate the suitable compression modulus for a dielectric that is suitable for the pressure range demanded for battery applications (Simplification: the compression modulus was assumed to be identical to the Young's modulus since there is more data available for the Young's modulus of materials).

$$E = \frac{\sigma}{\epsilon} \quad (2a)$$

with



$$\varepsilon = \frac{\Delta x}{x} \quad (2)$$

Based on discussions with partners from WP4 (NXP and Fraunhofer IISB), a sensible compression range that fulfils the safety criteria (no delamination of metal) but still gives enough change of capacitance to enable the required resolution of 1% over the measurement range (15 kPa) with a feasible read-out circuit was defined. Roughly 1-10% of compression ($\varepsilon = 0,01-0,1$) at full pressure (1500kPa) should be able to fulfil the criteria. With these two values, upper and lower limits for the Young's modulus of the dielectric material can be defined. The pressure of 1500 kPa can be seen as a stress σ . For this stress to result in a deformation of 10% (1%), a modulus E of 15 MPa (150 MPa) is needed. Conclusively, the material of choice should have a modulus in the range of 15-150 MPa. As it can be seen in figure 6, elastomers and rigid polymer foams fulfil this criterion – however as mentioned before, polymer foams are harder to manufacture and control. Furthermore, the second electrode would be difficult to manufacture on top of a porous material.

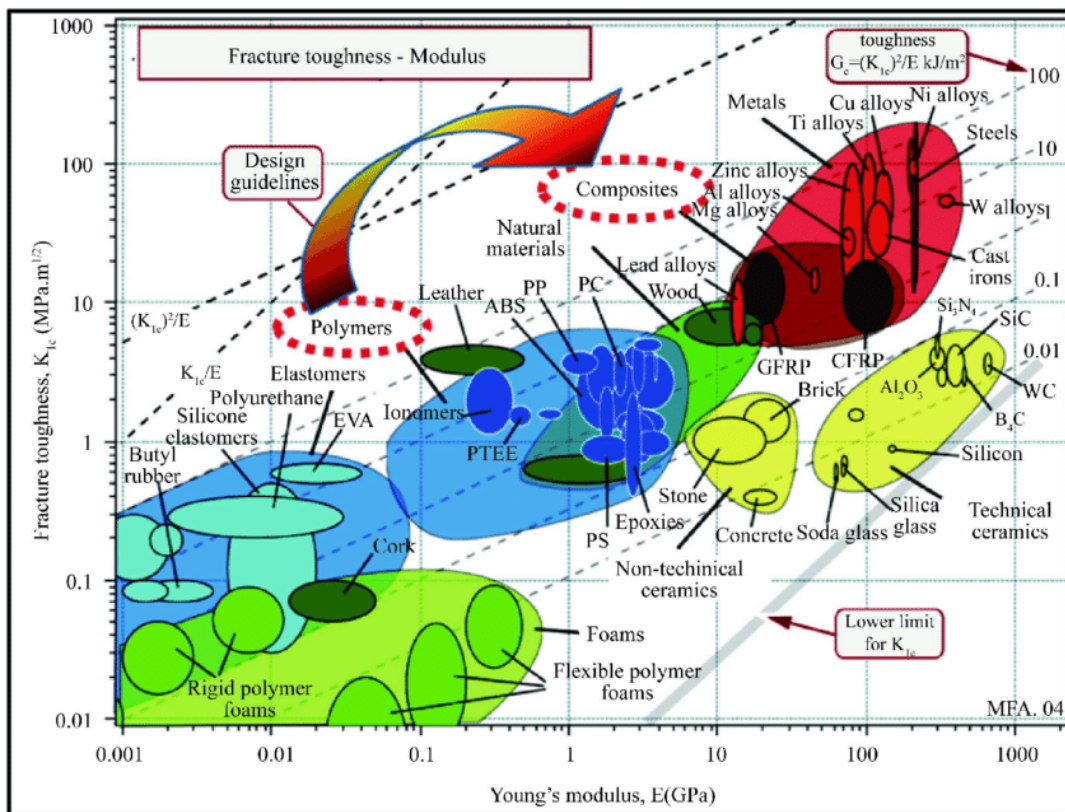


Figure 6: Comparison of the fracture toughness and Young's modulus values of polymers with other materials. [2]

Conclusively, the class of elastomers remains as option and a low viscosity two component polyurethane was chosen due to its suitable modulus and compatibility to the spin coating process, which is ideal for wafer level manufacturing and also is used for the polyimide substrate.

After optimization of spin coating parameters, adhesion promotion and homogeneity, first pressure sensors based on a polyurethane dielectric were manufactured and characterized via C-V-measurements (figure 7). To ensure better handling as well as more facile measurements under pressure, these first pressure sensors are processed as 20 mm x 20 mm large capacitors, which is well above the planed size of a single sensor in SENSIBAT's sensor matrix. Accordingly, absolute values for the capacitances should be taken with care and focus should be set on the sensitivity when looking at the presented measurements.



C-V-measurement under weight

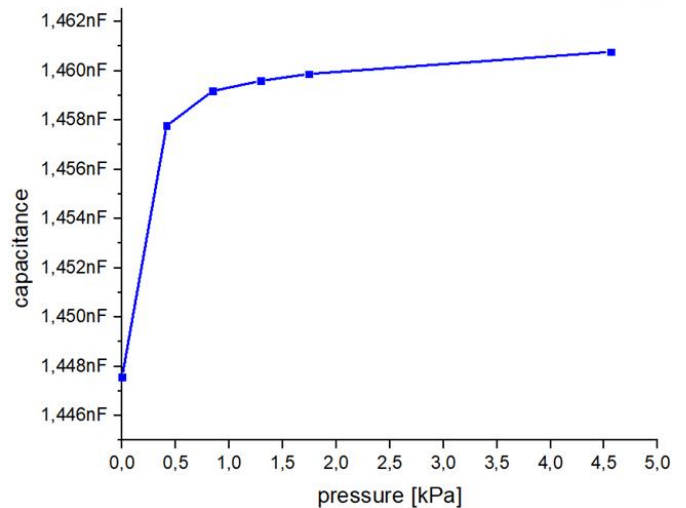
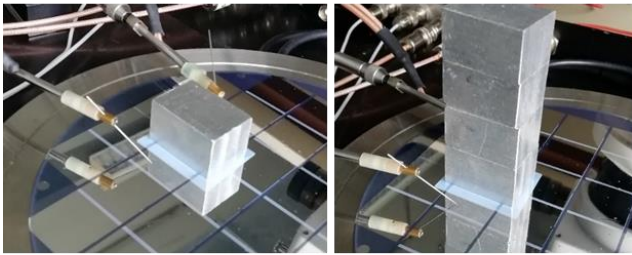


Figure 7: Initial measurement setup and results of PU-based pressure sensor characterisation under small loads.

For the first measurements, metal blocks were weighted and put on top of the capacitors to evaluate the dependency of the capacitance on the applied pressure. Within the linear regime ($>1\text{ kPa}$) a gain in capacity of $0,4\text{ pF/kPa}$ was measured, which corresponds to a change of $\sim 0,41\%$ per 15 kPa/m^2 (the defined minimum resolution).

Further pressure-dependent measurements were then performed with a different setup which can be seen in figure 8.

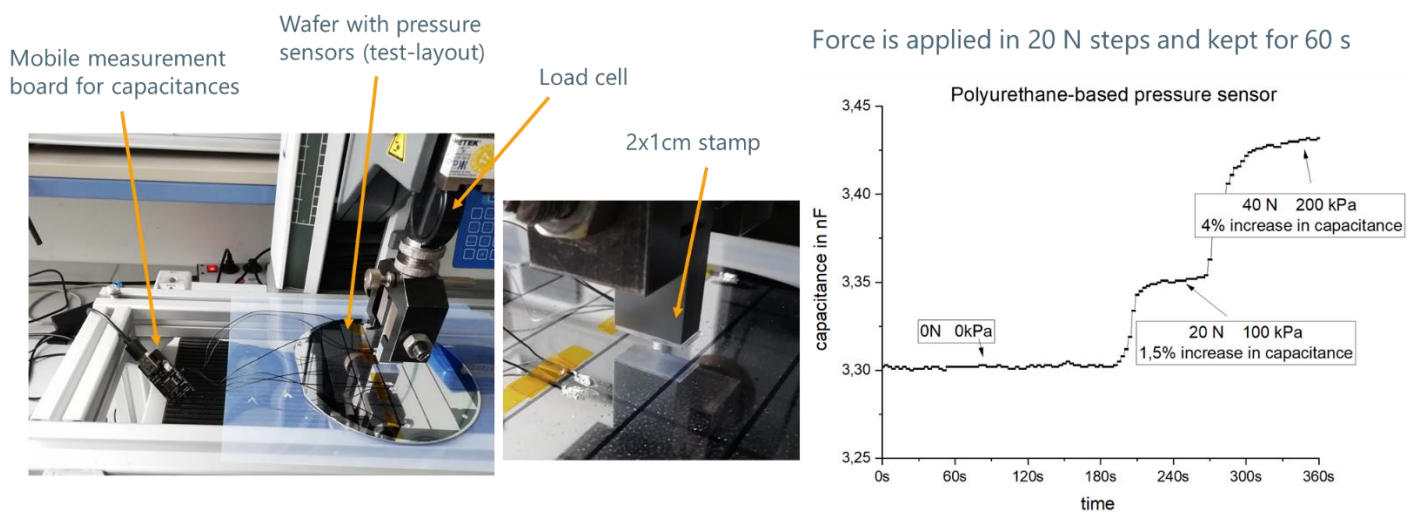


Figure 8: Advanced measurement setup and affiliated results for capacitive pressure sensors under higher loads.

With this setup, consisting of a mobile measurement board and a tensile testing machine, it was possible to evaluate the pressure sensors at higher loads. From the measurement curve in Figure 8 a change of approximately 4% for a pressure of 200 kPa ($0,3\%$ per 15 kPa) is evaluated which is slightly lower than estimated based on the first measurements with the weights. However, this change is still significant enough for a reliable measurement of the pressure within a cell.

Throughout the work done in parallelly conducted Task 3.3 it was evident that for proper adhesion of the encapsulation (parlylene-C) an annealing step of at least $120\text{ }^\circ\text{C}$ but ideally $200\text{ }^\circ\text{C}$ for several hours is of critical importance. Without this step, the barrier properties of the encapsulation are far inferior and failure of the whole



sensor matrix is likely. These findings will be further explained in Deliverable 3.3 but there is a critical connection to the development of the SENSIBAT pressure sensors: the polymer class of polyurethanes are generally speaking only stable and reliable for temperatures below 100 °C. This seems to be somehow contradictory to the requirement of short-term susceptibility to 140°C defined in D1.1. However, this requirement mainly is related to the hot-melt sealing at the edges of the cell or cell stack which is far off the regions where the pressure sensors will be placed in the final application. The datasheet of the specific polyurethane used as dielectric for the experiments above states a heat deflection temperature of 75°C (according to ISO 75B). Thermal degradation and loss of elasticity will take place within the material, if it is heated as it is needed for the parylene-C encapsulation.

Alternative, more heat stable dielectrics were consequently investigated: a silicone-based elastomers. The two silicone elastomers which were chosen and investigated (a “NuSil” elastomer by Avantor and a “Sylgard” elastomer by Dow) are mechanically and chemically stable for temperatures up to 275 °C and therefore suitable for the envisioned process flow.

After initial spin-coating optimizations - including thinning the highly viscous silicones in order to reduce the resulting layer thickness - homogenous and almost pinhole free dielectric layers could be achieved with the right set of process parameters, as it can be seen in Figure 9 (NuSil) and 10 (Sylgard). The SEM picture of the NuSil, which was taken after deposition of a nickel electrode, shows a silicone thickness of ~ 850 nm.

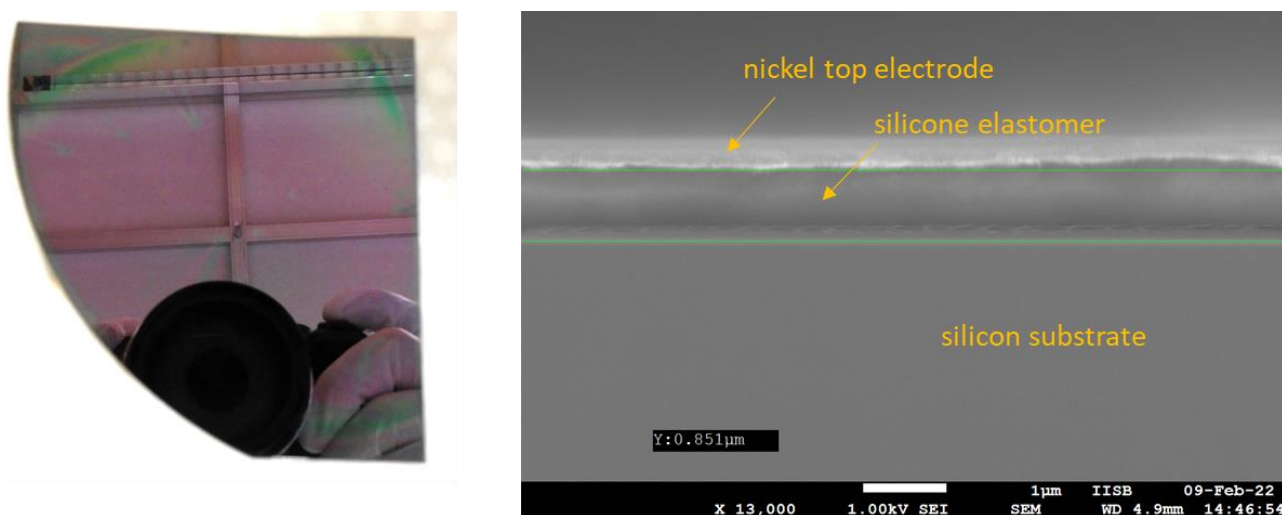


Figure 9: Photograph and SEM picture of NuSil dielectric on silicon substrate after initial optimisation of spin-coating process.

The optically transparent NuSil silicone has a red or greenish shine due to interference effects, which only appear when there is minor scattering of light. This indicates a smooth surface which is suitable for further processing. The smooth surface and homogeneity were also achieved for the Sylgard silicone (figure 10). Simple 20 x 20 mm capacitors were built through sputter deposition of a 300 nm thick metallization on top of the silicone and using the conductive substrate (highly doped silicon) as counter electrode for both silicone elastomers. Those structures were then used for an initial characterization regarding their material properties. Therefore leakage currents, base capacity measurements, frequency dependent measurements and voltage dependent measurements were performed to identify stable and reasonable parameters for the following characterization of the capacitors under pressure. Both the NuSil and Sylgard samples showed a base capacitance which is in good agreement with the measured thickness of the dielectric and the permittivity obtained from the materials data sheet.

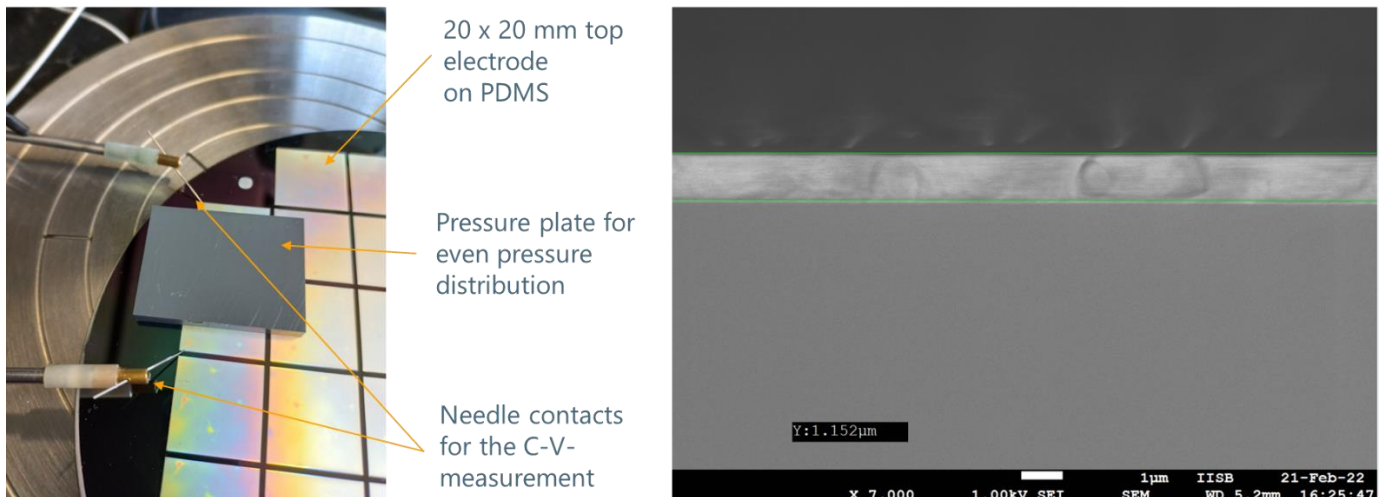


Figure 10: Photograph of test structures for pressure dependent characterisation based on Sylgard silicone (left) and SEM picture with thickness measurement of Sylgard on silicon wafer (right).

The Sylgard based capacitors unfortunately had high leakage currents, which made the correct interpretation of further measurements impossible. Those leakage currents were not to be expected based on the data sheet of the elastomer, however an influence of the solvent for dilution of the Sylgard precursor (which is used to get applicable thicknesses for the dielectric layers) might be the reason.

The NuSil based capacitors in return were manufactured on top of an additional layer of 50 nm Al_2O_3 . This additional insulation was used to improve the homogeneity and adhesion of the silicone, but also serves as additional barrier for currents, which can be seen in the leakage current measurements in figure 11.

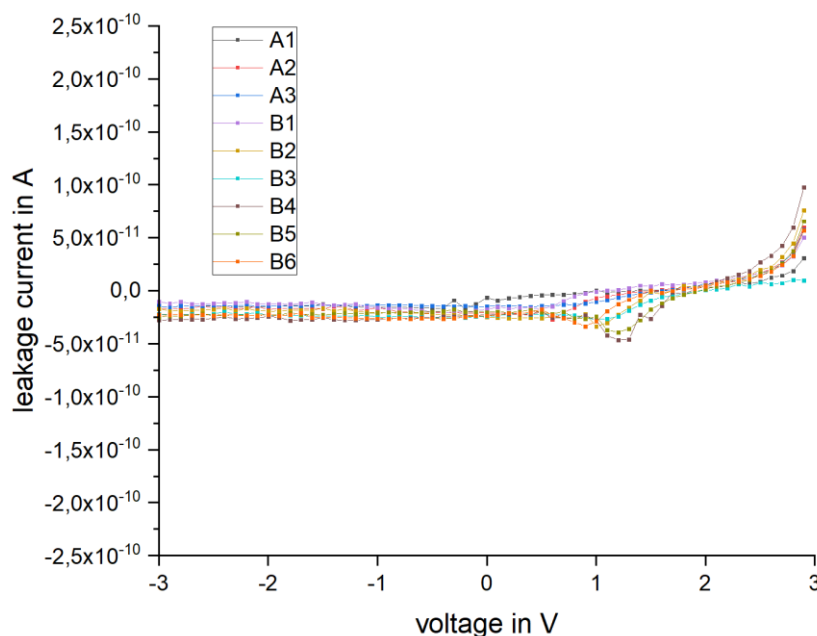


Figure 11: leakage current measurements for 9 NuSil capacitors between -3 and 3V.

The measured leakage currents are below 25 pA/cm^2 (which is around the detection limit of the used I-V measurement equipment and therefore can be interpreted as zero leakage). The breakthrough voltage of the



capacitors with this structure was determined to be around 45 V based on measurements with increasing voltages. Figure 12 shows the frequency dependence of the NuSil based capacitors.

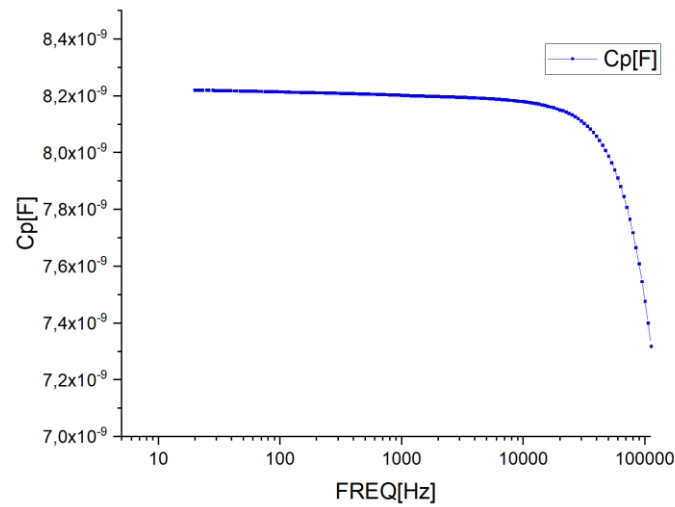


Figure 12: Frequency dependent measurement of the capacity of NuSil based test structures.

As can be seen in figure 12, the NuSil based capacitors show very stable capacitances of ~ 8,2 nF (lower absolute values to be expected for final layout due to smaller size) up to frequencies of around 20 kHz, while afterwards a continuous drop of the capacitance can be observed with increasing frequency. A measurement frequency of 1 kHz is therefore used for the further characterizations.

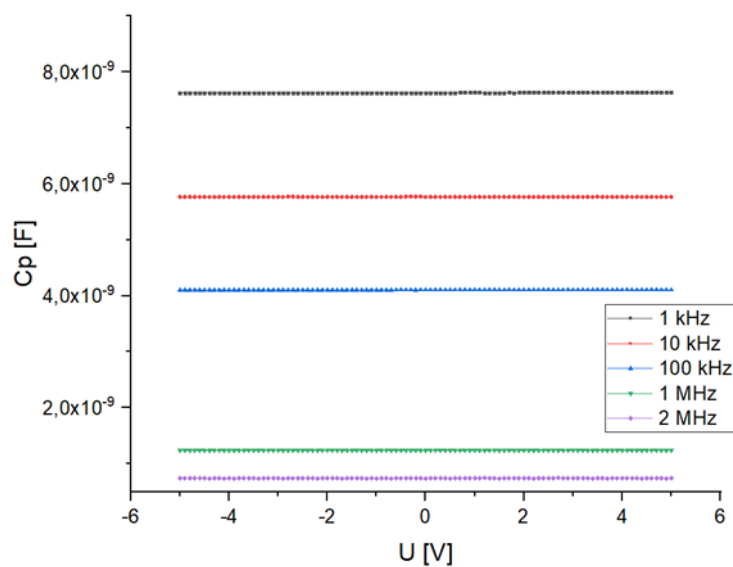


Figure 13: Voltage dependent measurement of the capacity of NuSil based test structures at different frequencies.

The voltage dependent measurement of a NuSil capacitor in figure 13 shows no voltage dependence of the measured capacitors between -5 and 5 V, which shows that no concerns are to be expected regarding the read-out voltage of the circuit which is developed within WP4 (the circuit will operate with the voltage of the battery).

First characterizations under pressure were performed with the setup shown in figure 14.

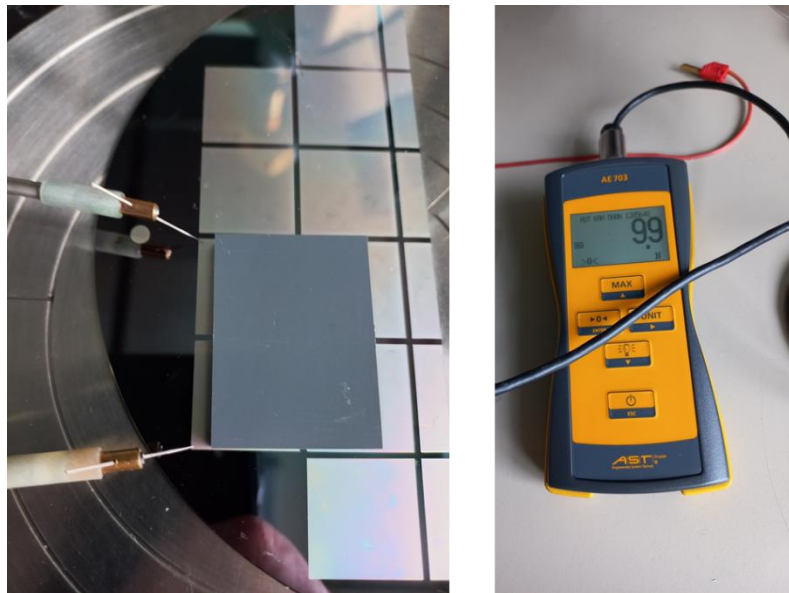


Figure 14: Equipment for initial characterisation of capacitors under pressure.

A polymer plate was used to apply uniform pressure onto the capacitors within a defined area (which is needed for the calculation of the pressure). The pressure is manually adjusted to fit defined steps with help of the load cell, while the capacitance is measured through the LCR-meter (plates are contacted through needles).

While there was a strong response to the manually applied pressure, the reason behind this response is unclear. The dimensions of the capacitance change do not match with the expected response based on the mechanical calculations, resulting in uncertainty regarding the sensitivity. Repeated leakage current measurements show that there is no significant increase in capacitor leakage though repeated application of pressures up to 300 kPa (higher pressures were not tested yet).

The volatility of the contact to the electrodes through needles, the rather thin (650 nm) compressible dielectric and the manual exertion of pressure have been identified as possible disruptive factors and will be investigated in ongoing experiments. Furthermore, the Sylgard will be also investigated in parallel with additional insulation (i.e. in sandwich structures) to prevent leakage currents. Additionally, plasma damage of the silicones through the metal deposition via sputtering is could be a factor influencing both silicone types and will be further examined.

Due to the relatively short-term adjustment of the pressure sensor dielectric, which is needed because of the annealing routine of the matrix encapsulation (Task 3.3), a conclusive evaluation of the pressure sensors is not possible at this point in time. However adjusted layouts to minimize the influence of the electrode contacts, additional layers to prevent leakage currents and more sophisticated setups to ensure a defined pressure onto the sensors while also ensuring a measurement of high resolution and without disturbances (not possible with the mobile measurement board shown in figure 8) are currently under investigation.



2.4 Integrated processing of temperature and pressure sensors

2.4.1 Process flow

The SENSIBAT sensor matrices are manufactured within a cleanroom with typical semiconductor processing methods like spin-coating, metallisation through vapor deposition, wet and dry etching and photolithography, which ensures high precision and reproducibility of fabrication. A simplified process flow is depicted in figure 15.

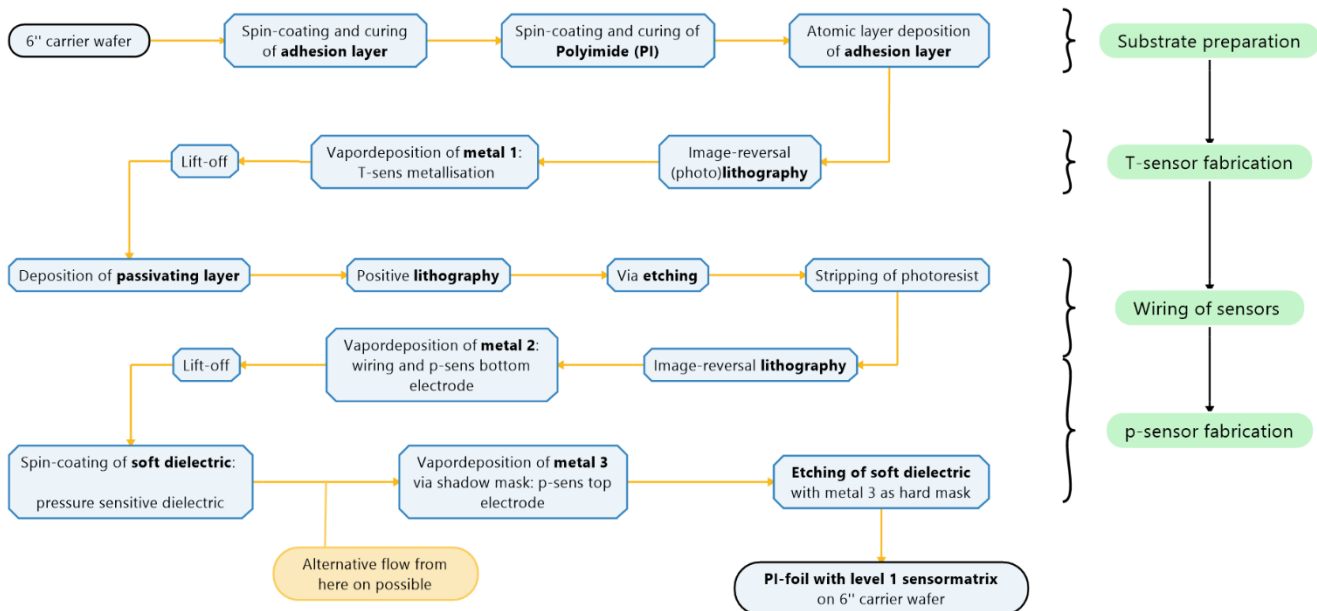


Figure 15: Process flow for the manufacturing of level 1 sensor matrices.

Note that the precise processing of the pressure sensors after deposition of the pressure sensitive dielectric is not yet fixed, since etching and metallisation options are still weighted against each other to ensure optimal performance of the pressure sensors and compatibility to the encapsulation (adhesion of the parylene). The interplay of the encapsulation and the sensor matrix is further discussed in Deliverable 3.3.

2.4.2 Wiring of sensor matrix

An important layout requirement for the sensor matrix is the interconnect technology to address each individual sensor of the matrix. Figure 16a shows the most straightforward approach where each sensor is connected by the respective number of connections (in this case two, as needed for a resistive or capacitive sensing element) and the connections are fed out of the matrix by avoiding crossings between the lines. It is clear that for a matrix of n rows and m columns a total number N of connectors will be required to contact the elements.

$$N = 2 \cdot n \cdot m \quad (3)$$

However, large numbers of wiring lines are hard to handle especially for large n and m values because of limited available space as well as unwanted distortion of the sealing line of the battery pouch by wide feed-through connectors.

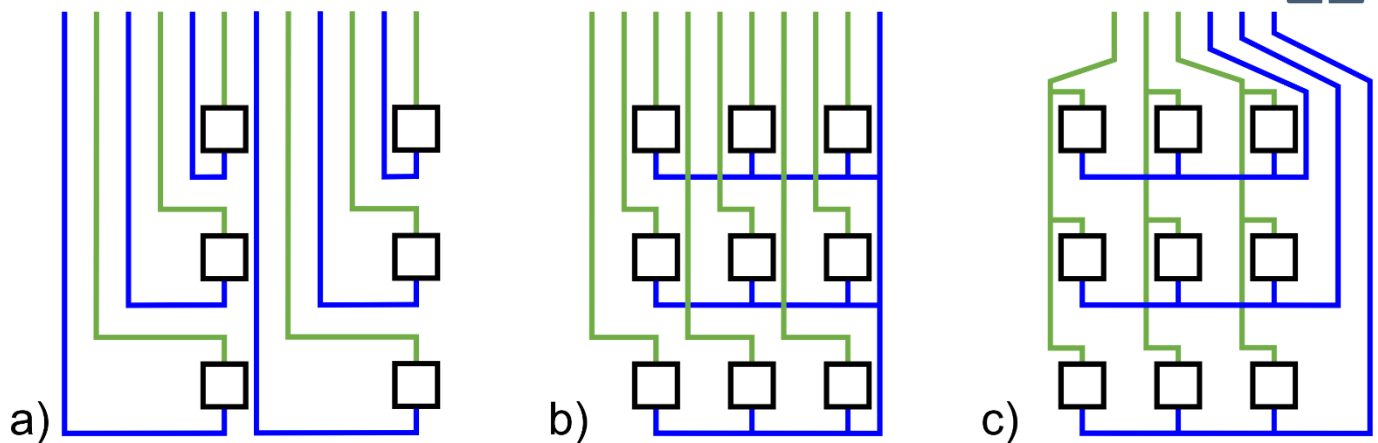


Figure 16: wiring schemes for contacting individual sensors in a matrix configuration. a) Contacting each element individually by the required number of wires. b) Common rail concept where all elements share a common ground or supply line. c) Cross point matrix where each row and each line share a single wire.

The number of lines can be reduced significantly, if there is one shared ground or supply line for all the elements, as depicted in Figure 16b. As an example, a single device can be read out by setting the forwarding (blue) line to a high voltage and measuring the respective current through the individual (green) reverse line of the element against ground. All other reverse lines should be driven in a way that does not deliver additional current contributions to the device of interest. In the given example this can be achieved by biasing them at a voltage the same or below the level of the forward line. In this case the total number of wires yields

$$N = n \cdot m + 1 \quad (4)$$

which is clearly below the number of lines in the first configuration. However, there are additional requirements with respect to biasing, as explained, and the technology must allow for crossing of the forwarding and reverse lines which demands an improved complexity and a low-leakage insulator between those two metals.

The maximum reduction of wires needed for addressing a matrix can be achieved when addressing all elements in a cross-point connection scheme (Figure 16c). As this has some advanced implications on the functionality of the matrix elements and the read-out data handling, it is only recommended for the addressing of large matrices. In this case the total number of wires yields

$$N = n + m \quad (5)$$

One major drawback of this approach is that all elements are shunted by parallel current paths that have to be controlled or accounted properly (Figure 17). A common approach is to use diodes in series with the sensing elements where this is technologically available. The rectifying behaviour will then block the parallel path at one or more points and suppresses the current through the shunting circuit. However, a rectifying or switching element is not available in the SENSIBAT application. Nevertheless, it is possible to evaluate the resistance of a single element by applying a dedicated scheme of measurement voltages to the respective lines and extracting the value of the targeted element by subsequent calculations. This procedure is selected in SENSIBAT for reading out the resistive temperature sensor matrix, whereas the capacitive read out of the pressure Sensors utilizes the common rail concept. The respective read-out schemes will be detailed in Deliverable 4.1 "Development of BMS-slave for module".

Figure 18 shows a photograph of a completely processed 1 Ah matrix of 12 temperature and 12 pressure sensors.

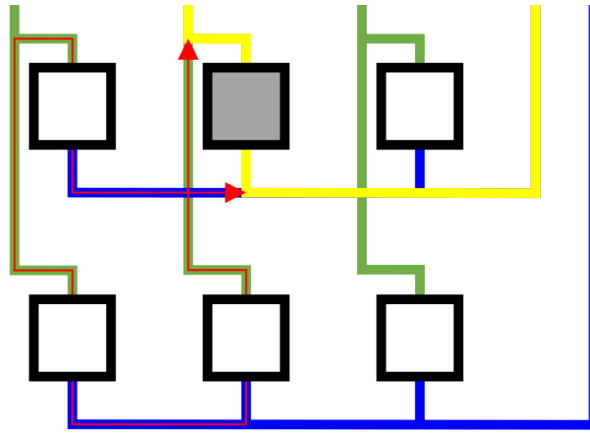


Figure 17: Parallel current paths in crosspoint configuration demand an advanced read-out scheme. The red path shunts reading out the element addressed by the yellow lines. Note that this is only one possible shunting path.

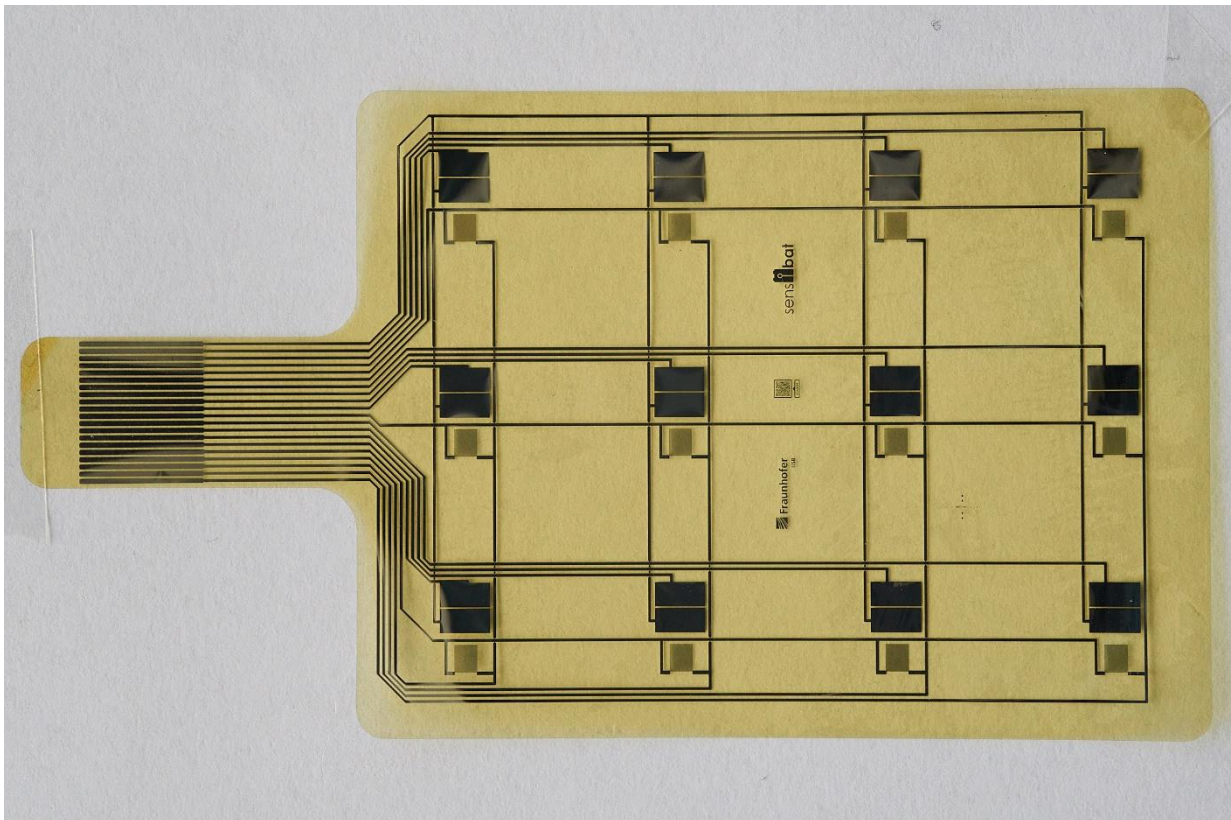


Figure 18: SENSIBAT Level 1 sensor matrix designed for 1 Ah battery cells before encapsulation. The matrix holds 12 resistive temperature sensors for cross-point array addressing as well as 12 capacitive pressure sensors in common rail configuration.



3 Discussion & Conclusion

The main objective of the deliverable is to proof the adaption and integration of established sensing concepts, i.e. the measurement of temperature by resistive elements and the capacitive detection of cell pressure for spatially resolved analysis of parameter distribution inside lithium-ion battery cells.

For realization of thermistors, three sensitive materials (Pt, Ni, NiAl) have been processed into resistive meanders and characterized. NiAl and especially Pt elements show the temperature sensitivity (TCRs) expected from literature values and offer low hysteresis in heating/cooling cycles and durability. Proper encapsulation of the resistive lines has been shown to be a prerequisite for achieving this good stability. The materials show good linearity and reproducibility in a temperature range of -20 °C to 120 °C. With respect to homogeneity, the samples show moderate variation that cannot be neglected for further data evaluation. As typical trimming or binning procedures are not feasible for the targeted application, the variations need for an initial matrix calibration and subsequent data handling algorithms in the battery management system.

Pressure sensitive parallel plate capacitors have been investigated for a range of compressible polymeric materials, of which polyurethane (PU) has proven the best performance covering detection of pressures in the range of several 100s of kPa as required by the application. Based on the achieved materials recipes, the functionality of the device designs and the integration capabilities could be proven.

The adapted device layouts for both temperature and pressure sensors and parallel considerations on sensor addressing together with SENSIBAT partners from WP4, responsible for read out of the sensor matrices, lead to the development of a wiring integration scheme and the realization of sensor matrix samples shown in Figure 18, targeting the 1 Ah cells of SENSIBAT. 18 matrices were produced and delivered to partners ABEE and VARTA for integration and performance tests.

As recent developments in Task 3.3 have elucidated, the encapsulation scheme for the matrices must include a high temperature annealing step (120°C to 200°C for 1 day) in oxygen-free atmosphere. Unfortunately, PU will not withstand temperatures above 100°C for longer times. Thus, the materials choice for the compressible insulator had to be revised. Polysilanes or polysiloxanes were identified as stable replacement offering sufficient electrical and mechanical properties and restarted the development cycle again. Due to the already established routes for device integration, the proven device design and the acquired knowledge in characterization techniques, we anticipate a significantly accelerated development cycle for this task and readiness of the fully-integrated matrices in time for the preparation of the sensor matrices for 5 Ah baseline cells due by M24. An according risk item was added to the risk table in Chapter 4 of this report.



4 Risks

| Risk No. | What is the risk | Probability of risk occurrence ¹ | Effect of risk ² | Solutions to overcome the risk |
|--------------------|---|---|-----------------------------|---|
| 1 – WP2/WP3 | <i>Sensors cannot withstand adverse environment in battery cell (e.g. may react with electrolyte to produce by-products) and lose sensitivity</i> | 3 | 1 | <i>A part of task 3.1 is focused on the encapsulation of the level 1 sensors for chemical resistance against electrolyte. The level 1 sensors will be integrated within a polymer substrate (PI) giving them an intrinsic (backside) encapsulation. An additional Parylene-C based conformal coating will be used to further protect the sensors against (electro-) chemical degradation. Due to its small thickness, this coating will only slightly shield the t-sensors from the heat and will still transduce the local pressure within the battery onto the p-sensors.</i> |
| 3 - WP3 | <i>Incompatibility of the sensors with the pouch cell assembly process</i> | 2 | 3 | <i>The level 1 sensors are chosen and designed to be as thin as possible to be compatible during the pouch cell assembly.</i> |
| 17 – WP3 | <i>Pouchbag cells are typically operated between two plates (braced together) – attached sensor may result in additional mechanical stress</i> | 2 | 2 | <i>Special design of the plates may become necessary, providing additional space for the attached sensor. The sensor matrices are kept as flat and thin as possible to minimize additional stress through the sensor. Additionally, the sensor matrix feed-through is placed at positions of the cell that do not interfere with the pressure plates (between the tabs for 1Ah cells and at the side for 5Ah cells).</i> |
| New - WP3x | <i>Silicone elastomer material will not show sufficient electrical/mechanical parameters for integration into capacitive pressure sensors</i> | 2-3 | 1 | <i>Investigation into 3 alternative materials in parallel</i> |

¹ Probability risk will occur: 1 = high, 2 = medium, 3 = Low

² Effect when risk occurs: 1 = high, 2 = medium, 3 = Low



5 References

- [1] Laurence W. McKeen, 1 - Introduction to Creep, Polymers, Plastics and Elastomers, Editor(s): Laurence W. McKeen, In *Plastics Design Library, The Effect of Creep and Other Time Related Factors on Plastics and Elastomers (Third Edition)*, William Andrew Publishing, 2015, Pages 1-41, ISBN 9780323353137, <https://doi.org/10.1016/B978-0-323-35313-7.00001-8>.
- [2] Atif, Rasheed & Inam, Fawad. (2016). Modeling and Simulation of Graphene Based Polymer Nanocomposites: Advances in the Last Decade. *Graphene*. 05. 96-142. 10.4236/graphene.2016.52011.



6 Acknowledgement

The author(s) would like to thank the partners in the project for their valuable comments on previous drafts and for performing the review.

Project partners

| # | PARTICIPANT SHORT NAME | PARTNER ORGANISATION NAME | COUNTRY |
|----|------------------------|---|-----------------|
| 1 | IKE | IKERLAN S. COOP. | Spain |
| 2 | BDM | BEDIMENSIONAL SPA | Italy |
| 3 | POL | POLITECNICO DI TORINO | Italy |
| 4 | FHG | FRAUNHOFER GESELLSCHAFT ZUR FOERDERUNG DER ANGEWANDTEN FORSCHUNG E.V. | Germany |
| 5 | FM | FLANDERS MAKE VZW | Belgium |
| 6 | TUE | TECHNISCHE UNIVERSITEIT EINDHOVEN | The Netherlands |
| 7 | NXP NL | NXP SEMICONDUCTORS NETHERLANDS BV | The Netherlands |
| 8 | NXP FR | NXP SEMICONDUCTORS FRANCE SAS | France |
| 9 | ABEE | AVESTA BATTERY & ENERGY ENGINEERING | Belgium |
| 10 | VAR | VARTA MICRO INNOVATION GMBH | Germany |
| 11 | AIT | AIT AUSTRIAN INSTITUTE OF TECHNOLOGY GMBH | Austria |
| 12 | UNR | UNIRESEARCH BV | The Netherlands |

DISCLAIMER/ ACKNOWLEDGMENT



Copyright ©, all rights reserved. This document or any part thereof may not be made public or disclosed, copied, or otherwise reproduced or used in any form or by any means, without prior permission in writing from the SENSIBAT Consortium. Neither the SENSIBAT Consortium nor any of its members, their officers, employees or agents shall be liable or responsible, in negligence or otherwise, for any loss, damage or expense whatever sustained by any person as a result of the use, in any manner or form, of any knowledge, information or data contained in this document, or due to any inaccuracy, omission or error therein contained.

All Intellectual Property Rights, know-how and information provided by and/or arising from this document, such as designs, documentation, as well as preparatory material in that regard, is and shall remain the exclusive property of the SENSIBAT Consortium and any of its members or its licensors. Nothing contained in this document shall give, or shall be construed as giving, any right, title, ownership, interest, license, or any other right in or to any IP, know-how and information.

This project has received funding from the European Union's Horizon 2020 research and innovation programme under grant agreement No 957273. The information and views set out in this publication does not necessarily reflect the official opinion of the European Commission. Neither the European Union institutions and bodies nor any person acting on their behalf, may be held responsible for the use which may be made of the information contained therein.